Supplementary Information

1. The conversion efficiency and mode purity of SPP, VWP and VVP

The common way to generate a LG mode is to add the spiral phase to a Gaussian mode using a q-plate, a SPP, and so on (i.e., the extracavity configuration) [51]. The generated mode can be expressed as

$$e^{-\left(\frac{r}{w_0}\right)^2}e^{-il\phi} = \sum_p c_{lp}\mathrm{LG}(l,p). \qquad (S1)$$

In comparison to the standard LG mode

$$\mathrm{LG}(l,p) = \sqrt{\frac{2p!}{\pi(p+|l|)!}}\frac{1}{w_0}\left(\frac{\sqrt{2}r}{w_0}\right)^{|l|}L_p^{|l|}\left(\frac{2r^2}{w_0^2}\right)\times e^{-\left(\frac{r}{w_0}\right)^2}e^{-il\phi}. \qquad (S2)$$

one can see that the necessary amplitude term to define a pure LG mode is missing in Eq. (S1). Therefore, directly adding a spiral phase to the Gaussian mode as in Eq. (S1) will generate a superposition of various higher-order LG modes rather than a pure LG mode [37, 52, 53].

For a SPP, its conversion efficiency corresponds to the directly generated mode (Eq. (S1)), while the mode purity is the ratio of a pure LG(l, 0) mode (Eq. (S2)) to the directly generated mode (Eq. (S1)). Table S1 shows the conversion efficiencies of commercial SPPs (data obtained from the website of the companies) and the measured mode purities under extra-cavity configuration by using the standard modal decomposition method [14, 37]. Figure S1 shows the output patterns under extracavity and intracavity configurations.

Table S1 | Comparisons of various commercial spatial phase plates

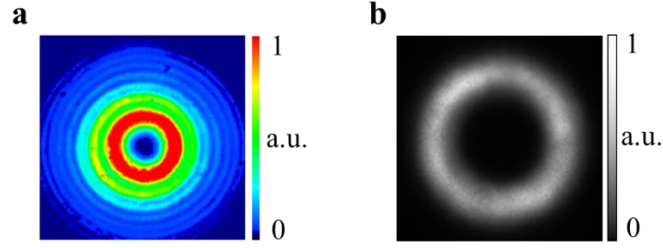| Components and Target LG(l, p) mode	Spiral phase plate (l=1) LG(1, 0)	Zero-order vortex half-wave retarders (l=1) LG(1, 0)	Vector vortex Waveplates l=1, 2, 4		
			LG(1, 0)	LG(2, 0)	LG(4, 0)
Manufacturer	HOLO/OR Ltd.	Thorlabs Inc.	BEAM Co.		
Conversion efficiency (provided by manufacturer)	>95%	>97%	>95%	>95%	>95%
Mode purity	<80% [Ref. S3]	<80% [Ref. S5]	86%	84%	72%

Fig. S1 | Mode pattern under (**a**) extracavity configuration (obtained from Thorlabs Inc., https://www.thorlabs.com/newgrouppage9.cfm?objectgroup_id=9098) and (**b**) intracavity configuration. Here, $l = 4$ for both patterns.

2. The dependence of output signal wavelength on PPLN channel and temperature.

A traditional optical parametric oscillator (OPO) using a PPLN crystal converts a pump wave into a signal wave and an idle wave. The three waves satisfy the energy conservation, i.e., $\omega_p = \omega_s + \omega_i$, where ω_p, ω_s, and ω_i refer to the frequencies of the pump, signal, and idle waves, respectively. By changing the temperature and channel of the PPLN crystal, ω_s and ω_i can be tunable due to the momentum conservation condition $\vec{k_p} - \vec{k_s} - \vec{k_i} - \vec{G} = 0$, where $\vec{k_p}$, $\vec{k_s}$, and $\vec{k_i}$ refer to the wave vectors of the pump, signal, and idle waves, respectively [31, 54]. $\vec{G}$ is the first-order reciprocal vector provided by the PPLN crystal. In our experimental setup, the PPLN crystal has ten channels. We use four channels with periods of 31.02 μm, 30.49 μm, 29.98 μm, and 29.52 μm, respectively, as shown in Fig. S2. Under the pump wavelength of 1064 nm, the output signal wavelengths can be tuned from 1480 nm to 1650 nm in the temperature ranging from 25°C to 138°C (Fig. S3).
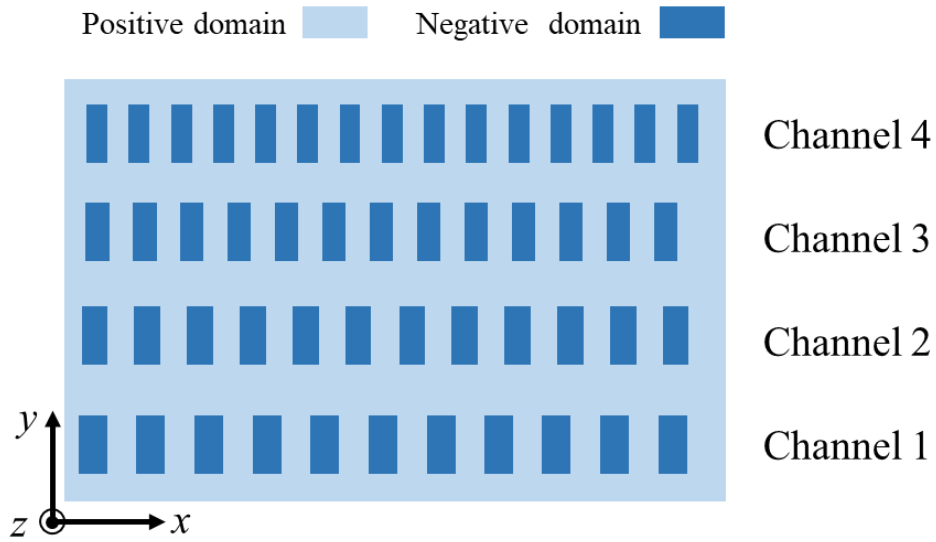
Fig. S2 | Schematic image of four channels in the PPLN crystal. The periods are 31.02 μm, 30.49 μm, 29.98 μm, and 29.52 μm, corresponding to Channel 1, 2, 3, and 4, respectively.
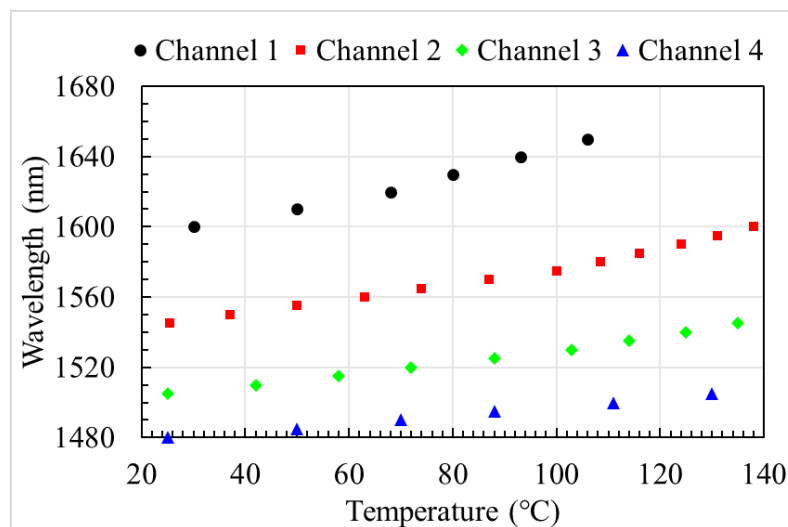

Fig. S3 | The dependence of output signal wavelength on PPLN channel and temperature.

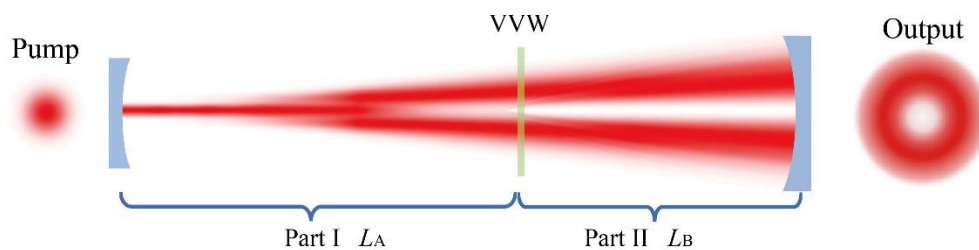## 3. Mathematical analysis of Janus OPO

Fig. S4 | The Janus cavity design.

The Janus cavity mode features two faces, i.e., a Gaussian-shape profile near the input coupler and a single high-purity LG(l, $p = 0$) mode on the output coupler, as shown in Fig. S4. The l index is determined by VVW. In the following, we will mathematically analyze the Janus cavity design.

In order to simplify the process, the cavity is divided into Part I (from the input coupler to VVW) and Part II (from VVW to the output coupler). Since the target is to output a pure LG mode, we assume only a single LG(l, 0) mode at the output coupler. Its propagation is generally defined by

$$
\begin{aligned}
\mathrm{LG}\left(l, p = 0, z\right) = &\sqrt{\frac{2}{\pi\left(1+|l|\right)!}}\frac{w_0}{w(z)}\left(\frac{\sqrt{2}r}{w(z)}\right)^{|l|}\exp\left(-\frac{r^2}{w^2(z)}\right)\times \\
&\exp\left(-il\varphi\right)\exp\left(-\frac{i\pi r^2}{\lambda R(z)}\right)\exp\left(i\psi(z)\right)
\end{aligned}
\tag{S3}
$$

Here, λ is wavelength, ω_0 is the beam waist, r and φ are the radial and azimuthal coordinates, respectively, $w(z)$ is the beam size, $R(z)$ is the radius of curvature, and $\psi(z)$ is the Gouy phase.

It should be noted that the imaging system in Janus cavity will introduce an additional diverging curvature into the cavity mode. To guarantee the cavity self-consistency, the evolving curvature of the LG mode should be coincident with the mirror surface at the output coupler [55]. Taking into account the additional curvature from the imaging system, we assume that the beam waist of the LG mode in Part II is at a distance of $L + L_B$ relative to output coupler. Then, one can obtain the curvature radius of the output coupler R_{OC}

$$
R_{\mathrm{OC}} = R\left(L + L_B\right) = \left(L + L_B\right)\left[1 + \left(\frac{\pi\omega_0^2}{\lambda\left(L + L_B\right)}\right)^2\right].
\tag{S4}
$$

When the LG beam in Part II passes through VVW, the spiral phase is cancelled and the generated beam can be expressed as LG(l,0)exp($il\varphi$), i.e.,

$$
U = \sqrt{\frac{2}{\pi\left(1+|l|\right)!}}\frac{w_0}{w(L)}\left(\frac{\sqrt{2}r}{w(L)}\right)^{|l|}\exp\left(-\frac{r^2}{w^2(L)}\right)\exp\left(-\frac{i\pi r^2}{\lambda R(L)}\right).
\tag{S5}
$$

Notably, the beam in Eq. (S5) is quite close to a hollow-Gaussian beam [50], which will evolve to a Gaussian-like beam after a certain propagation distance.

In our design, Part I is an imaging system. The input coupler with a curvature of R_{IC} is equivalent to a lens with a focusing length of $f = R_{\mathrm{IC}}/2$. In our experiment, we employ a symmetric imaging system, in which VVW is placed at curvature center of the input coupler. Therefore, after the beam defined by Eq. (S5) is reflected by the input coupler, its image field can be written as

$$
U_I\left(u, v\right) = \iint_S h\left(u, v; \xi, \eta\right)U\left(\xi, \eta\right)d\xi d\eta,
\tag{S6}
$$

with

$$h(u,v;\xi,\eta) = \exp\left[\frac{i\pi}{\lambda R_{IC}}(u^2+v^2)\right]\exp\left[\frac{i\pi}{\lambda R_{IC}}(\xi^2+\eta^2)\right]\delta(\xi+u,\eta+v). \tag{S7}$$

Substituting Eq. (S7) into Eq. (S6), one can get

$$U_I(u,v) = \exp\left[\frac{i2\pi}{\lambda R_{IC}}(u^2+v^2)\right]U(-u,-v). \tag{S8}$$

The cavity reversible condition requires

$$U_I(u,v) = U^*(u,v), \tag{S9}$$

By substituting Eqs. (S5) and (S9) into Eq. (S8) and considering $r^2 = u^2 + v^2$, one can obtain

$$R_{IC} = R(L) = L\left[1+\left(\frac{\pi\omega_0^2}{\lambda L}\right)^2\right]. \tag{S10}$$

Based on Eqs. (S4) and (S10), one can solve the necessary parameters ω_0 and L to determine the Janus cavity mode.

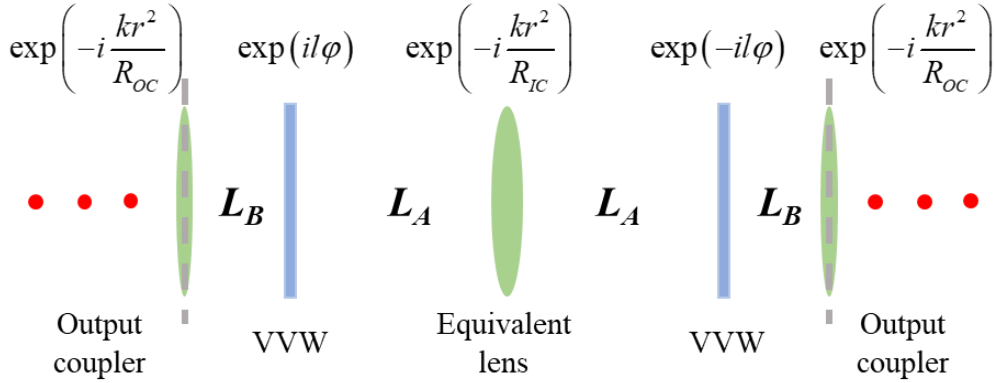## 4. Janus cavity mode simulation

Fig. S5 | One round trip in Janus cavity. The transmittance functions of the used optical components are shown. In our experiment, R_{IC} =75 mm, R_{OC} = 125 mm, and L_B =55 mm.

The numerical simulation is carried out using Fox-Li iterative procedure. Figure S5 shows one round trip in Janus cavity. The propagation between the optical components is calculated by the angular spectrum theory [56].

Based on the Fox-Li method, we simulate the Janus cavity mode with VVWs of $q = 0.5$, 1, and 2, which can generate LG(1,0), LG(2,0), and LG(4,0) modes, respectively. The one-round-trip transitions of Janus cavity mode are shown in Fig. S6. The symmetric imaging system facilitates the cavity mode to smoothly evolve from a Gaussian profile to an LG profile, and vice versa, without breaking the cavity mode reversibility. The simulated output modes show the intensity and phase of

the LG mode can be well reconstructed after a round trip inside the Janus cavity. Notably, the imaging system introduces a diverging curvature, which is taken into account in the self-reproductive Janus cavity mode (See Supplementary Note 3). In addition, the measured beam sizes are well consistent with the theoretical and simulated values as shown in Table S2. One can perform similar calculations to analyze the cavity mode without an imaging system (Fig. 1d of the main text).
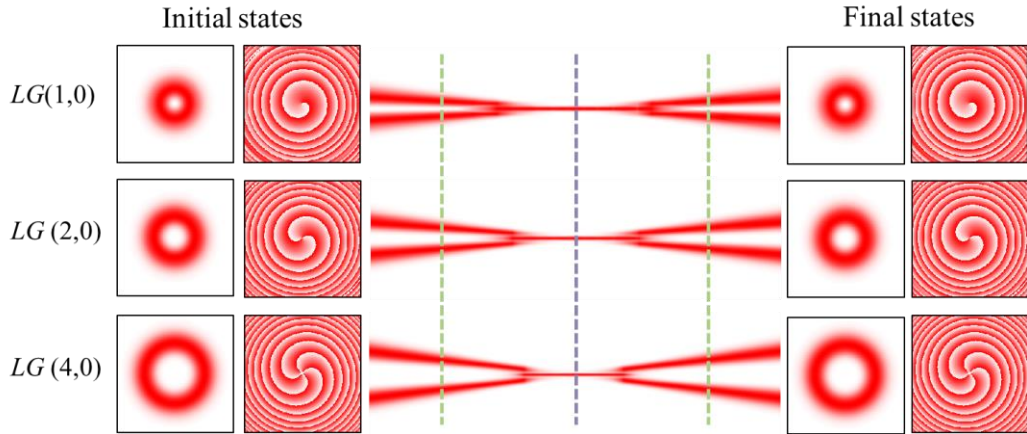

Fig. S6 | One-round-trip mode conversions inside Janus cavity for generating LG(1,0), LG(2,0), and LG(4,0) modes, respectively.

Table S2 | Comparison of beam sizes in experimental, theoretical, and simulating results.

| | Output beam sizes at a far-field distance of d from the output coupler | | |
	$l=\pm1, d=110$ mm	$l=\pm2, d=90$ mm	$l=\pm4, d=40$ mm
Experimental results	2.27 mm	3.19 mm	3.34 mm
Theoretical results	2.39 mm	3.09 mm	3.35 mm
Simulating results	2.37 mm	3.03 mm	3.35 mm

Figure S7 show that the intensity profiles for pump mode and various TC orders inside the crystal. In principle, to guarantee an ideal Janus cavity mode for different VVWs, the pump beam should be re-optimized to match the intensity profile for a particular TC at the input coupler. However, by using a 200 μm pump beam size in our experiment, the mode purity and conversion efficiency slightly changes as the TC varies from 1 to 4. It should be noted that the cavity parameters need to be re-optimized if the TC becomes far away from this range.
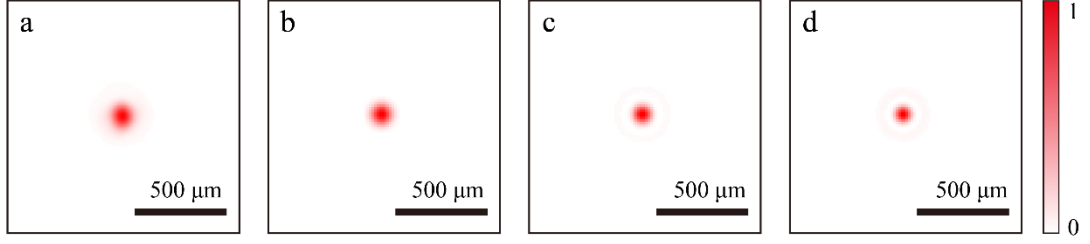
Fig. S7 | (a) The experimental intensity pattern of pump mode; **(b-d)** Simulated Gaussian-like modes corresponding to the outputs of LG(1,0), LG(2,0) and LG(4,0) modes, respectively.

5. Working principle of VVW and reversible polarization conversion

A VVW can be seen as a spatially variant half-wave plate, whose optical axis rotates continuously around a singularity point. Its transmissivity is up to 95% covering wavelengths from 1500 nm to 1600 nm. The orientation of its fast axis can be expressed as:

$$\theta(\varphi)=q\varphi+\varphi_0, \tag{S11}$$

where φ is the variant azimuthal angle, φ_0 is the orientation of the fast axis at $\varphi=0$ and q is a constant with its value of being positive multiple of 1/2. Its Jones Matrix can be written as:

$$J_q(\theta)=\begin{bmatrix} cos\,2\theta & sin\,2\theta \\ sin\,2\theta & -cos\,2\theta \end{bmatrix}. \tag{S12}$$

When a circularly polarized beam passes through the VVW, the following transformation happens [57],

$$\begin{cases} J_q(\theta)\times|l_0, & L\rangle=|l_0+m, & R\rangle \\ J_q(\theta)\times|l_0, & R\rangle=|l_0-m, & L\rangle \end{cases}, \tag{S13}$$

where L and R refer to the left-circularly-polarized (LCP) and right-circularly-polarized (RCP) states, respectively. From Eq. (S13), we can see that a LCP (or RCP) state with TC of l_0 passing through the VVW will become a RCP (or LCP) state with TC of l_0+2q (or l_0-2q). When a $l_0=0$ input state is used, the TC will be controlled by the $2q$ value of the VVW, i.e. $l=2q$, and the handedness of the incident circularly-polarized beam.

In the experiment, a broadband quarter-wave plate (QWP) is used to convert the generated linearly-polarized signal wave into a circularly-polarized one. The Jones matrix of QWP can be expressed as

$$G_{\pi/2}(\beta) = \frac{\sqrt{2}}{2} \begin{bmatrix} 1 - i\cos 2(\beta - \beta_0) & -i\sin 2(\beta - \beta_0) \\ -i\sin 2(\beta - \beta_0) & 1 + i\cos 2(\beta - \beta_0) \end{bmatrix}. \tag{S14}$$

where β and β_0 is the orientation angle of the fast axis of QWP and the polarization angle of the signal wave, respectively. Consider that a light beam propagates forward through QWP and VVW, is reflected by the output coupler, and then propagates backward through VVW and QWP. The process can be expressed by,

$$\begin{aligned} J_{total}(\theta, \ \beta) &= G_{\pi/2}(-\beta) J_q(-\theta) J_m J_q(\theta) G_{\pi/2}(\beta) \\ &= -2i \begin{bmatrix} \cos 2(\beta - \beta_0) & \sin 2(\beta - \beta_0) \\ -\sin 2(\beta - \beta_0) & \cos 2(\beta - \beta_0) \end{bmatrix}. \end{aligned} \tag{S15}$$

J_m is the Jones Matrix describing the mirror reflection, which is given by

$$J_m = \begin{bmatrix} 1 & 0 \\ 0 & -1 \end{bmatrix}. \tag{S16}$$

Note that the right-hand coordinate system requires the azimuthal angle to change its sign when the light wave propagates backward.

It requires $\beta - \beta_0 = \pm 45°$ for transforming a linearly-polarized state into a circularly-polarized state. So one can obtain from Eq. (S15) that the polarization is rotated by $\pm 90°$ after the light passes through QWP and VVW forward and backward. We use a Faraday rotator (FR) to compensate the $\pm 90°$ polarization rotation so that the total polarization conversion process is reversible as shown in Fig. S8.
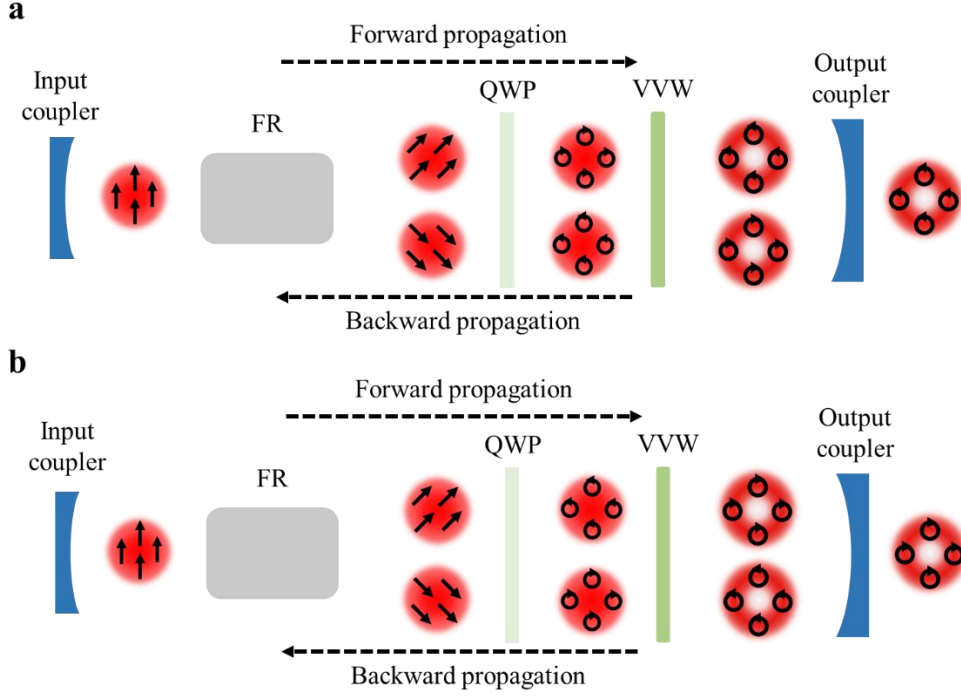
Fig. S8 | Polarization and mode conversions inside the Janus OPO cavity for outputs of (**a**) right-circularly-polarized $LG(2q,0)$ mode and (**b**) left-circularly-polarized $LG(-2q,0)$ mode. The value of q is positive multiple of 1/2. The solid arrows indicate the polarization while the dash arrows show the propagation directions.

6. Modal analysis process.

Modal decomposition using digital holograms is a common way to characterize the spatial beams [37]. Because all the LG_l^p modes construct a complete and orthonormal basis, the spatial mode $U(x, y)$ can be expanded into the coherent superposition of LG_l^p modes:

$$U(x,y) = \sum_{l=-\infty}^{\infty} \sum_{p=0}^{\infty} c_l^p LG_l^p(x,y). \tag{S17}$$

Here, c_l^p is the weighting coefficient, which can be calculated from

$$c_l^p = \langle LG_l^p(x,y) | U(x,y) \rangle = \iint U(x,y) LG_l^p(x,y)^* \, dxdy. \tag{S18}$$

$LG_l^p(x, y)^*$ is the complex conjugate of $LG_l^p(x, y)$. To simplify the calculation, we apply a Fourier transform on $U(x, y) \cdot LG_l^p(x, y)^*$,

$$U_k(k_x, k_y) = \iint U(x,y) LG_l^p(x,y)^* \exp\left[-i(k_x x + k_y y)\right] dxdy, \tag{S19}$$

where the k_x and k_y are the wave vectors. Then, the on-axis optical field in the Fourier plane is given

by

$$U_k(0,0)=\iint U(x,y)LG_l^p(x,y)^* \, dxdy . \tag{S20}$$

Therefore, by measuring the intensity of $U_k(0,0)$, the power weighting of the corresponding LG_l^p component can be determined by

$$\left|c_l^p\right|^2 = \left|U_k(0,0)\right|^2 . \tag{S21}$$

Equation (S21) provides a practical way to determine the mode purity of the spatial mode.

In the experiment, we use a reflective phase-only spatial light modulator (SLM, GAEA-2 - TELCO, HOLOEYE Corporation) to perform the modal analysis. We use the type-3 method of complex-amplitude modulation reported by Arrizon et al. to program the phase-only computer-generated holograms (CGH) [58]. A spatial carrier frequency is added into the CGH so that the 1st order diffraction beam (which reconstructs the conjugate of the tested LG_l^p component) is separated from the undesired modes in the Fourier plane.

Figure S9 shows the schematic setup for the modal decomposition. Because the SLM is only valid for linearly-polarized light, we turn the output circularly-polarized LG mode into a linearly-polarized one by using a QWP. Then it passes through a 1:1 beam splitter (BS) and is incident on the SLM. The light field reflected at SLM and BS in sequence carries the information of $U(x,y)LG_l^p(x,y)^*$, which is focused by a 75 mm lens to perform the Fourier transform. At the Fourier plane, the first-diffraction-order beam reconstructs the field $U_k(k_x,k_y)$, which is picked out through an iris and is imaged on the laser beam profiler by a 50X objective. By recording the central intensity of the image, the power weighting is achieved. In the experiment, we measure the modal distribution of the generated LG_1^0 beam by loading a group of LG_l^{p*} modes with p varying from 0 to 4 and l varying from 0 to 2, onto the SLM.
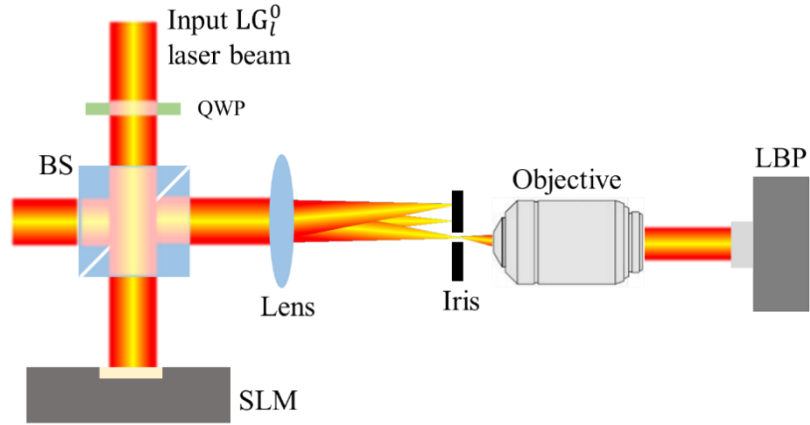
Fig. S9 | The schematic setup for modal decomposition.

7. The influences of cavity collimation and cavity length on mode purities

In our configuration, the singularity of VVW should collimate with the optical axis of two-mirror cavity to ensure generation of high-purity LG modes. Figure S10 shows the influence of misalignment on the mode purity of LG(1,0) mode based on numerical simulation. As the singularity of VVW moves away from the optical axis, the output LG(1,0) mode distorts with a reduce in mode purity and finally evolves into a Gaussian mode. In experiment, the VVW is fixed on a manual translation stages with the accuracy of 10 μm to guarantee precise collimation.

The cavity length L should satisfy the stability condition of $0 < \left(1 - L/R_1\right)\left(1 - L/R_2\right) < 1$, where R_1 and R_2 are the curvature radius of the mirrors, so that its accuracy depends on the value of R_1 and R_2 in centimeter scale [48]. However, one should note that the cavity length will change the spot size of signal Gaussian-like modes in the PPLN crystal.
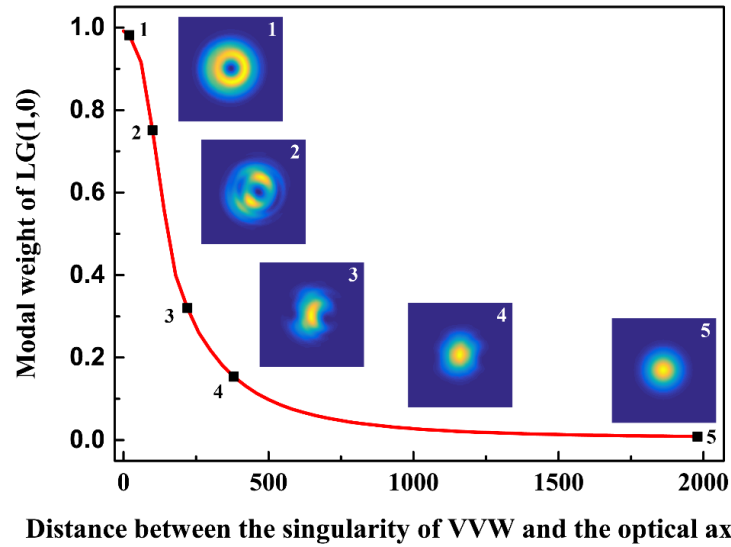
Fig. S10 | The modal weighting of LG(1,0) dependence on the distance between the singularity of VVW and the optical axis. Insets are the output intensity patterns corresponding to certain distances.

8. The linewidth of output LG mode

Figure S11 shows the measured linewidth of the pump and the output signal modes, in which the full width at half maximum (FWHM) are of 5 nm for the pump mode and 1.4 nm for the signal mode, respectively. Replacing with a CW pump laser, it is possible to generate narrow-linewidth LG modes that could be used to investigate spin-orbital coupling with various atoms in quantum applications.
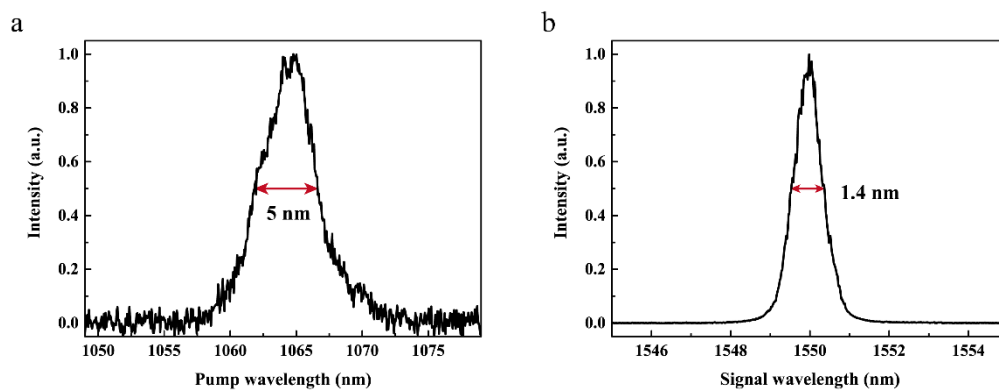

Fig. S11 spectra of **(a)** the pump mode and **(b)** the signal mode centered at 1550 nm .